Effect of quantum-mechanical symmetry on the geometric structures of intrashell states of three-valence-electron atoms

C. G. Bao
Department of Physics, Zhongshan University, Guangzhou, 510275 People's Republic of China

C. D. Lin
Department of Physics, Kansas State University, Manhattan, Kansas 66506-2601

(Received 15 May 1995)

The effect of quantum-mechanical symmetry on the geometric structures and internal motions of the intrashell states of three-valence-electron atoms is investigated with a model where the core and all the radial degrees of freedom of the valence electrons are frozen. A number of correlative densities have been defined and calculations have been carried out for the eight $N=2$ intrashell states of boron as examples. For each state, the most probable shape, the preference of orientation, and the favorable modes of internal motion have been found.

PACS number(s): 31.10.+z, 32.80.Dz, 31.25.−v

I. INTRODUCTION

The nature of electron-correlation in two-electron atoms has been widely investigated ([1–4], and literature cited therein) in the past decade and is now well understood [5]. However, investigation of correlation in three-electron atoms is only at a primitive stage [6–9]. Because of the additional three degrees of freedom, compared to the two-electron atoms, the nature of correlation in three-electron systems is expected to be much richer and much more complicated. In fact, collective internal modes arising from the correlated motion of three electrons have already been partially analyzed [7]. (This reference is denoted as WL hereafter.) This paper examines the geometric structures of P and D states. Study for S states has been carried out previously [10,11]. Emphasis is placed on the discovery of the geometric structure and internal motion by analyzing the wave functions of several intrashell states. Such a qualitative study is desirable in order to obtain a global picture and a possible new classification of the complicated spectra of three-electron systems.

In two-electron atoms, it was found that classification schemes [4,12,13] that are suitable for intrashell states are also approximately suitable for intershell states. This implies that an understanding of internal modes of intrashell states is important for understanding the whole spectrum. For this reason, we shall concentrate on intrashell states in this paper. In particular, the intrashell states of boron where the three valence electrons stay in the $N=2$ shell are the object of this study.

Two approximations are adopted. (i) The degrees of freedom of the core electrons are frozen. Since we consider only cases where the core is completely filled, this approximation is reasonable. (ii) The radial degrees of freedom of the valence electrons are frozen. This is called an r-frozen model, which has already been used before (WL), and in two-electron atoms [14]. In intrashell states the radial part of the wave function is totally symmetric with respect to permutations of electrons; this symmetry is strictly reserved in the r-frozen model. Thus our model does not spoil the quantum-mechanical (QM) symmetry. In fact, as we shall see, the basic structures of the lower states (of a given $^{2S+1}L^{\pi}$) are essentially determined by the QM symmetry, but not by the details of dynamics; in particular, these structures are expected to hold also for other three-valence-electron systems (e.g., the triply excited intrashell states of Li, the $N=3$ intrashell states of Al, . . . ,etc.).

II. DESCRIPTION OF THE THEORETICAL MODEL

By freezing the radial degree of freedom of the three electrons, the Hamiltonian of the model atom reads

$$H=\frac{\hbar^2}{2mr_0^2}\sum_{i=1}^{3}\hat{l}_i^2+e^2\sum_{i>j}\frac{1}{|\vec{r}_i-\vec{r}_j|}, \tag{1}$$

where $\hat{l}_i$ is the angular-momentum operator of each electron (e_i) with respect to the nucleus and $\vec{r}_i$ is its position vector from the center, $\vec{r}_i=r_0\hat{r}_i$. The r_0 is taken to be 0.776 Å to simulate the $N=2$ shell of boron [15]. The calculated eigenvalues below depend on the choice of r_0; however, the order of the eigenvalues stays the same and the nature of the eigenstates is not changed.

The eigenvalues of the model Hamiltonian (1) are obtained by diagonalization in a basis set consisting of functions

$$\tilde{\Phi}_i=\mathscr{A}(\{[l_1(\hat{1})l_2(\hat{2})]_{l_0}l_3(\hat{3})\}_{LM}\chi^s_{SM_S}). \tag{2}$$

where $\mathscr{A}$ is the antisymmetrizer, and the basis function is written as the product of the total orbital angular function coupled to L and M and the total spin function $\chi^s_{SM_S}$ coupled to S and M_S. The coupling scheme is such that the first two electrons couple to an intermediate l_0, which then couples with the third electron to L, and the spins of the first two electrons couple to an intermediate s, which then couples with the third spin to S. It is noted that the $\tilde{\Phi}_i$'s do not form

TABLE I. Eigenenergies of $N=2$ intrashell states of boron from an r-frozen model. The energy is in eV, the energy of the ground state, $^2P^o$, is scaled as zero.

State	$^2P^o$	$^4P^e$	$^2D^e$	$^2P^e$	$^2S^e$	$^4S^o$	$^2D^o$	$^2P^o(2)$
E_i	0	7.26	12.71	19.70	19.71	24.35	24.44	30.59

an orthonormal set; among them only mutually linearly independent basis functions can be reserved in the model space.

Let each of the l_i's be constrained by $0 \leq l_i \leq l_{\max}$; then the dimension of the model space is determined by $l_{\max}$. In what follows $l_{\max}=3$ is given. From the point of view of the independent-electron model, $l_{\max}$ is simply equal to 1 in the $N=2$ shell. The $l_{\max}$ has been given a larger value since the electron-electron repulsion may increase the orbital angular momentum of each electron. For the $N=2$ intrashell states, a contribution from l_i greater than 3 is not expected to change the qualitative features of the relevant states.

After diagonalization, eigenstates Ψ_i of different $^{2S+1}L^{\pi}$ symmetries are obtained. Among them, it is found that there are only eight states that have coefficients dominated by basis functions where all the components have $l_i \leq 1$. These eight states are identified as the eight $N=2$ intrashell states of boron, and the wave function of each state will be analyzed below.

The eigenenergies of the eight states and their $^{2S+1}L^{\pi}$ labels are listed in Table I. These states are the lowest states for each $^{2S+1}L^{\pi}$ symmetry, except for the last one where (2) was used to indicate that it is the second state of that symmetry. Although the r-frozen model cannot give accurate energy levels, the relative order of the calculated positions of all the eight states coincides with the experimental levels for C^+ [16], except that the order for $^2P^e$ and $^2S^e$ is reversed. We compare the calculations with the data for C^+, since the positions of all the eight states are known and the r-frozen model is expected to work better for positive ions where the intershell correlation is smaller. We mention that the positions of all these eight intrashell states for boron and for He^- have not been determined unequivocally yet [17]. This calculation also disagrees with WL, where the two states $^2S^e$ and $^2P^e$ were found to be at much higher energies.

Definition of one-body and two-body density functions

For $S=1/2$ states, the spin-up and spin-down electrons play different roles in structure; thus a polarity-dependent procedure of analysis is used. Each eigenstate is expanded as

$$\Psi=\sum_i C_i\tilde{\Phi}_i=\sum_{\mu} f_{\mu_1\mu_2\mu_3}(\hat{1}\hat{2}\hat{3})\xi_{\mu_1}(1)\xi_{\mu_2}(2)\xi_{\mu_3}(3), \tag{3}$$

where $\xi_{\mu_i}(i)$ is the spin state of e_i with polarity $\mu_i=\pm 1/2$, and Σ_{μ} implies a summation over μ_1, μ_2, and μ_3 under the constraint $\mu_1+\mu_2+\mu_3=M_S$. Owing to the antisymmetrization, we have

$$f_{\mu_1\mu_2\mu_3}(\hat{1}\hat{2}\hat{3})=(-1)^p f_{\mu_{p_1}\mu_{p_2}\mu_{p_3}}(\hat{p}_1\hat{p}_2\hat{p}_3) \tag{4}$$

where $p_1p_2p_3$ is a permutation of 123 and $(-1)^p$ is the permutation parity. Equation (4) implies that different $f_{\mu_1\mu_2\mu_3}$ components would provide equivalent information; thus the *analysis of only one component is sufficient.* In what follows, $M_S=1/2$ and $M=L$ are assumed. With this choice we have two spin-up electrons and one spin-down, and L is essentially lying along the Z axis; thus the anisotropy, which will be discussed later, is in fact relative to the direction of L. Mostly, the $f_{\frac{1}{2}\frac{1}{2}\bar{\frac{1}{2}}}$ is selected for analysis; with this choice the spins of e_1 and e_2 are up, while e_3 is down.

Let the normalization condition be written as

$$1=\sum_{\mu}\int d\hat{r}_1 d\hat{r}_2 d\hat{r}_3 |f_{\mu_1\mu_2\mu_3}|^2. \tag{5}$$

Then one can define the polarity-dependent one-body densities $\rho_{\uparrow}$ and $\rho_{\downarrow}$ as

$$\rho_{\uparrow}(\hat{r}_1)=\sum_{\mu}\delta_{\mu_1\frac{1}{2}}\int d\hat{r}_2 d\hat{r}_3 |f_{\mu_1\mu_2\mu_3}|^2, \tag{6}$$

$$\rho_{\downarrow}(\hat{r}_1)=\sum_{\mu}\delta_{\mu_1\bar{\frac{1}{2}}}\int d\hat{r}_2 d\hat{r}_3 |f_{\mu_1\mu_2\mu_3}|^2, \tag{7}$$

where $\rho_{\uparrow}(\hat{r}_1)$ $[\rho_{\downarrow}(\hat{r}_1)]$ is the probability density of having an up [down] electron at $\hat{r}_1$; in fact, it depends only on θ_1 but not on ϕ_1. The sum of $\rho_{\uparrow}$ and $\rho_{\downarrow}$ is just the usual total one-body density, fulfilling

$$1=2\pi\int \sin\theta_1 d\theta_1(\rho_{\uparrow}+\rho_{\downarrow}). \tag{8}$$

To define two-body densities, let $f_{\mu_1\mu_2\mu_3}$ be decomposed as

$$f_{\mu_1\mu_2\mu_3}=\sum_q C_q^{\mu}\{[l_1(\hat{1})l_2(\hat{2})]_{l_0}l_3(\hat{3})\}_{LM}, \tag{9}$$

where q denotes a partial wave channel ($l_1l_2l_3$ and l_0), and μ denotes $\mu_1\mu_2\mu_3$. Let us introduce a body frame E', so that the third body axis $\vec{k}'\|\vec{r}_1\times\vec{r}_2$, and the first body axis $\vec{i}'\|(\vec{r}_1+\vec{r}_2)/2$. Let $\alpha'\beta'\gamma'$ denote the Euler angles specifying the orientation of the E' frame; then Eq. (9) can be rewritten as

$$f_{\mu_1\mu_2\mu_3}=\sum_K D^L_{KM}(-\gamma',-\beta',-\alpha')G_{\mu K}, \tag{9'}$$

where

$$G_{\mu K}=\sum_q C_q^{\mu}\{[l_1(\hat{r}_1')l_2(\hat{r}_2')]_{l_0}l_3(\vec{r}_3')\}_{LK}, \tag{10}$$

where the three vectors with respect to the E' frame are $\hat{r}_1'=(\pi/2,-\theta_{12}/2)$; $\hat{r}_2'=(\pi/2,\theta_{12}/2)$, where θ_{12} is the angle between $\vec{r}_1$ and $\vec{r}_2$; and $\hat{r}_3'=(\theta_3',\phi_3')$. It is clear that $G_{\mu K}$ is a function of θ_{12} and $\hat{r}_3'$. The condition of normalization reads

$$1=\sum_{\mu}\int d\mathscr{R}\,\sin(\theta_{12})d\theta_{12}d\hat{r}_3'\left|\sum_K D^L_{KM}G_{\mu K}\right|^2, \quad (11)$$

where $d\mathscr{R}=\sin\beta' d\alpha' d\beta' d\gamma'$ denotes an infinitesimal rotation.

From Eq. (11), one can define the *orientation-averaged spin-parallel weighted two-body density* as

$$\tilde{\rho}_{\uparrow\uparrow}(\theta_{12})=\sin(\theta_{12})\int d\mathscr{R}\,d\hat{r}_3'\left|\sum_K D^L_{KM}G_{\mu_\alpha K}\right|^2, \quad (12)$$

where μ_α denotes $\mu_1=1/2$, $\mu_2=1/2$, and $\mu_3=-1/2$. Similarly, the spin-antiparallel two-body density is defined as

$$\tilde{\rho}_{\uparrow\downarrow}(\theta_{12})=\sin(\theta_{12})\int d\mathscr{R}\,d\hat{r}_3'\left(\left|\sum_K D^L_{KM}G_{\mu_b K}\right|^2+\left|\sum_K D^L_{KM}G_{\mu_c K}\right|^2\right), \quad (13)$$

where μ_b denotes $\mu_1=1/2$, $\mu_2=-1/2$, and $\mu_3=1/2$; μ_c denotes $\mu_1=-1/2$, $\mu_2=1/2$, and $\mu_3=1/2$. Evidently, the sum of the above two densities is the usual two-body densities

$$\tilde{\rho}_2=\tilde{\rho}_{\uparrow\uparrow}+\tilde{\rho}_{\uparrow\downarrow}, \quad (14)$$

fulfilling

$$1=\int d\theta_{12}\tilde{\rho}_2. \quad (15)$$

Furthermore, from Eq. (11) a polarity-dependent orientation-distribution function can be defined as

$$\rho_{\rm ori}^{\mu_1\mu_2\mu_3}=\int \sin(\theta_{12})d\theta_{12}d\hat{r}_3'\left|\sum_K D^L_{KM}G_{\mu k}\right|^3, \quad (16)$$

which is a function of β' and γ' (but does not depend on α'). This function gives *the distribution of the orientation of the E' frame*, where the X'-Y' plane is defined by the two electrons having polarity μ_1 and μ_2.

In what follows, the above defined functions will be inspected. Owing to particle-particle correlation, the distribution of a wave function in the multidimensional coordinate space is far from uniform but distributed around some most probable shapes; in this sense the geometric structure can be defined. Besides, in $L\neq 0$ states, the orientation of a geometric structure relative to L is relevant. Furthermore, each state has its most preferable modes of internal motion. The most probable shape, the most preferable orientation, and the most preferable mode of motion characterize the geometrical and dynamical features of quantum states. Before presenting the details, let us first inspect the effect of symmetry.

III. SYMMETRY CONSIDERATION

A. The existence of inherent nodal surfaces

It is natural that in the head state (the lowest state of a given $^{2S+1}L^{\pi}$ symmetry), the valence electrons would pursue a geometric structure with the best symmetry for reducing the total potential energy. For the present three-electron systems, the better choice is a coplanar (all three valence electrons together with the core staying in a plane) isosceles triangle (IST) configuration [including the equilateral triangle (ET)]. Thus the head state would pursue this configuration, and the wave function would be expected to be smoothly distributed (without nodes) around it; this optimal configuration can be defined as the most probable shape. On the other hand, quantum-mechanical symmetry can impose inherent nodal surfaces (INS's) in the multidimensional coordinate space, depending on the $^{2S+1}L^{\pi}$ symmetry [18–20]. The distribution of the wave functions of the head states would avoid the INS's since the nodal surfaces would induce a specific mode of motion resulting in an increase of kinetic energy. Hence, the most probable shape of the head states would possess not only a superior geometric symmetry, but would also do its best to avoid the INS's. In what follows, we shall neglect the discussion of $L=0$ states, as they have been discussed elsewhere [10,11].

B. Quantum symmetry imposed on the lying coplanar IST

Let the plane of the three electrons be denoted by σ and assume an IST configuration. When σ is lying in the X-Y plane, it is called a lying coplanar IST; when σ contains the Z axis, it is called an upstanding coplanar IST. When $L\neq 0$, a coplanar IST would have a smaller rotational kinetic energy than an upstanding IST, since the moment of inertia of the former relative to the Z axis is roughly twice that of the latter. However, in any coplanar structure, a space inversion is equivalent to a rotation in the σ plane by 180°. Hence, if σ lies in the X-Y plane, the coplanar configuration is an INS for all the $\pi(-1)^L=-1$ states. Thus, among the six $L\neq 0$ intrashell states shown in Table I, only $^2P^o$, $^2P^o(2)$, and $^2D^e$ states can have the lying coplanar IST as their most probable shapes.

C. Quantum symmetry imposed on the upstanding coplanar IST

Next we inspect the stability of changing the orientation of the lying coplanar IST. Assume that the up electrons e_1 and e_2 are located symmetrically on the two sides of the X axis, as shown in Fig. 1(a), and r_{12} is the base of the IST. A rotation about the X axis would turn the lying IST to an upstanding IST, as shown in Fig. 1(b). However, in Fig. 1(b), a space inversion together with a rotation about the Z axis by 180° is equivalent to an interchange of $\vec{r}_1$ and $\vec{r}_2$. Since both e_1 and e_2 are spin-up, the latter operation definitely provides a (-1) factor in the wave function. Accordingly, this upstanding IST has a node for all $\pi(-1)^L=+1$ states. For this reason, the $^2P^o$, $^2P^o(2)$, and $^2D^e$ states would avoid having $\vec{r}_{12}$ parallel to the Z axis.

D. Inclination of the IST

Another possible variation of the IST is its inclination, as shown in Fig. 1(c). When the angle of inclination is equal to

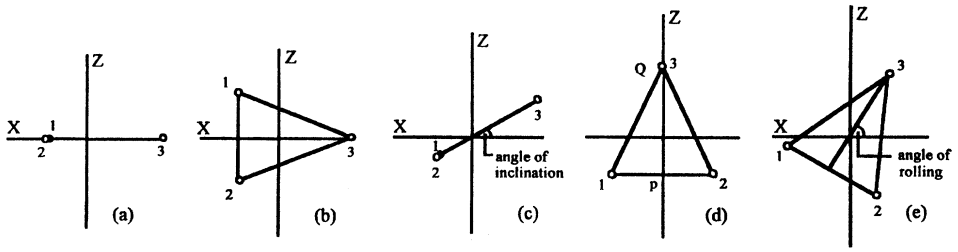

FIG. 1. Coplanar IST configuration of the valence electrons. The two electrons located at the base vertexes are spin-up, while the one at the top is spin-down. In (a) and (c), the two electrons at the base are overlapped. The Z axis is parallel to L.

90°, the lying IST is again changed to an upstanding IST with pQ [shown in Fig. 1(d)] overlapping with the Z axis. In this case a rotation about the Z axis by 180° is equivalent to an interchange of $\vec{r}_1$ and $\vec{r}_2$; thus an INS appears in $L=$even states. For this reason, the $^2D^e$ state would tend not to have a strong inclination.

From the above analysis, we predict that both $^2P^o$ and $^2D^e$ states prefer the lying coplanar IST. The IST may incline from the X-Y plane with the base $\vec{r}_{12}$ preferably normal to L. The tendency of inclination is stronger in the P state, but weaker in the D state. Thus, in the $^2D^e$ state, the three electrons are better kept close to the X-Y plane, while in the $^2P^o$ state the down-electron has a better chance of being close to the poles due to inclination.

The $^2P^o(2)$ state may also tend toward the lying coplanar structure. However, an energetic excited state is in general less constrained by the symmetry, and thereby less well predicted.

On the other hand, since the $\pi(-1)^L=-1$ states are prohibited from possessing the lying coplanar structure, it is natural that they would pursue an upstanding coplanar IST. With this choice, $\vec{r}_{12}$ may be either parallel to the Z axis [shown in Fig. 1(b)] or normal to it [Fig. 1(d)]. The former orientation is acceptable for all $\pi(-1)^L=-1$ states; the latter is acceptable only in those with $L=$odd. Starting from Fig. 1(b), if the IST rotates about the Y axis, as shown in Fig. 1(e), it is called a rolling. Among all the $\pi(-1)^L=-1$ states, the $L=$even states would prefer not to have a strong rolling.

From this analysis, we predict that all the $^4P^e$, $^2P^e$, and $^2D^o$ states tend toward the upstanding coplanar IST. The plane of this IST may roll about its normal; however, in the $^2D^o$ state $\vec{r}_{12}$ is better kept parallel to L. The above predictions arise simply from symmetry; they will be checked against results from the actual calculations.

IV. ONE-BODY DENSITIES

Among the functions defined in Sec. II, we first examine the polarity-dependent one-body densities, Eqs. (6) and (7). These densities are shown as a function of θ_1 in the upper frames of Fig. 2 for the $\pi(-1)^L=+1$ intrashell states and in the lower frames for the $\pi(-1)^L=-1$ states (the two $L=0$ states are not given here since they are isotropic). Figure 2 shows the differences between the $\pi(-1)^L=+1$ and -1 states and between $\rho_\uparrow$ and $\rho_\downarrow$ in $S=1/2$ states. A "typical" $\pi(-1)^L=+1$ state is $^2D^e$ [Fig. 2(c)] where all the electrons tend to lie in the X-Y plane, as predicted and as displayed in Fig. 1(a). For the two $^2P^o$ states, as shown in Figs. 2(a) and 2(b), the up electrons also prefer to lie on the X-Y plane, but the down electron may be close to the pole as the result of inclination [Fig. 1(c)]. (Recall that the inclination is larger for the $^2P^o$ states, see Sec. III D.) A typical $\pi(-1)^L=-1$ state is the $^2D^o$ state [Fig. 2(g)] where the two up electrons tend to be close to the poles, while the down electron remains in the X-Y plane [Fig. 1(b)] as predicted based on the symmetry in Sec. III. In Fig. 2(f) the down electron may be close to the pole because of the rolling [Fig. 1(e)].

For $S=3/2$ [Fig. 2(e)] the up and down electrons play exactly the same role; thus $\rho_\uparrow=2\rho_\downarrow$.

We have also investigated one $^2F^o$ state. This is not an intrashell state, but rather an intershell state. Note that its distribution, or symmetry, is similar to that of the $^2P^o$ and $^2D^e$ states.

V. ORIENTATION-DISTRIBUTION FUNCTIONS

We next consider the orientation distribution function. Especially we examine $\rho_{\rm ori}^{\frac{1}{2}\frac{1}{2}\frac{1}{2}}$ as functions of β' and γ', where e_1 and e_2 have their spins up and stay in the X'-Y' plane and the positive side of the X' axis. Our goal is to show the difference in the $\pi(-1)^L=+1$ states (shown on the left side of Fig. 3) from the $\pi(-1)^L=-1$ states (shown on the right side of Fig. 3).

There are four noticeable regions in the (β',γ') plane: the first region has $\beta'\approx 0$, $\gamma'=$any, where $\vec{r}_{12}$ lies in the fixed X-Y plane as in Fig. 1(a); the second region has $\beta'=$any, $\gamma'\approx 0°$ or 180°, where $\vec{r}_{12}$ may leave from the

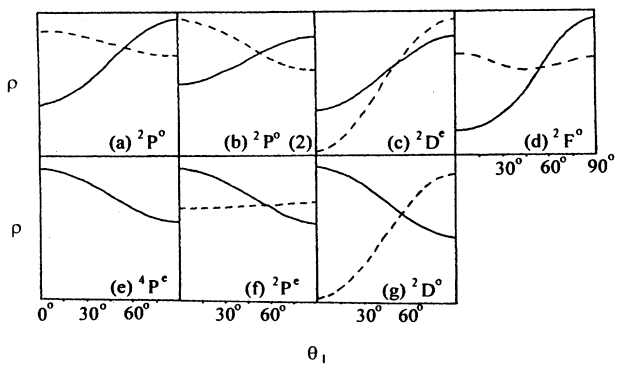

FIG. 2. Polarity-dependent one-body densities $\rho_\uparrow$ and $\rho_\downarrow$ as functions of θ_1. $M=L$ and $M_s=1/2$ are assumed. $\rho_\uparrow/2$ is given by the full line; $\rho_\downarrow$ by the dashed line. The ordinate in each figure is in arbitrary units.

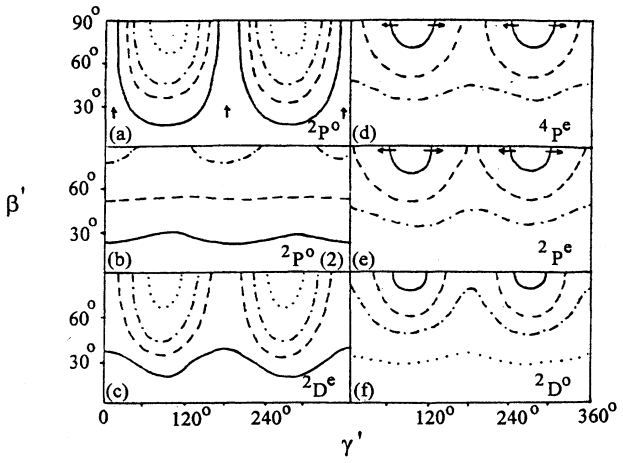

FIG. 3. Orientation-distribution functions $\rho^{\frac{1}{2}\frac{1}{2}\frac{\bar{1}}{2}}_{\text{ori}}$. The full line gives 92% of the maximum, the dashed lines give 72%, the dashed-dotted line gives 52%, while the dotted lines give 20%.

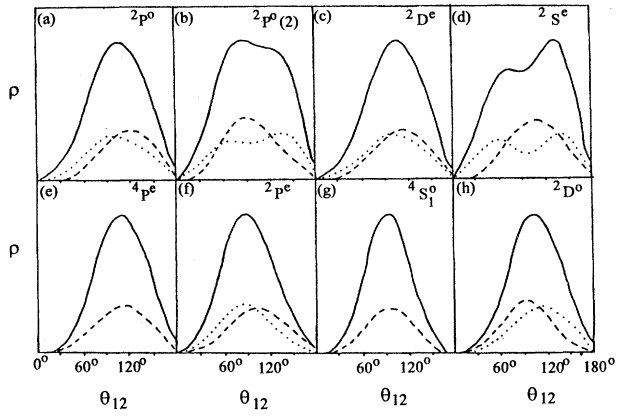

FIG. 4. Two-body densities as functions of θ_{12} (the angular separation of e_1 and e_2). The dashed line is for $\tilde{\rho}_{\uparrow\uparrow}$, the dotted line is for $\tilde{\rho}_{\uparrow\downarrow}/2$, and the full line is for $\tilde{\rho}_2=\tilde{\rho}_{\uparrow\uparrow}+\tilde{\rho}_{\uparrow\downarrow}$. The ordinate in each figure is in arbitrary units.

X-Y plane, but remains normal to the Z axis [the variation of β' is associated with inclination as shown in Fig. 1(c)]; the third region has $\beta'\approx 90°$, $\gamma'\approx 90°$, where $\vec{r}_{12}$ is parallel to the Z axis, as in Fig. 1(b); the fourth region has $\beta'\approx 90$, $\gamma'=$ any, where the variation of γ' is associated with rolling as in Fig. 1(e).

In the $^2D^e$ state, if the coplanar IST is lying as predicted, $\vec{r}_{12}$ should lie in the X-Y plane; thus the first region should be preferred, which is clearly the case shown in Fig. 3(c). In the $^2P^o$ state, if the coplanar IST is allowed to incline, then not only the first region but also the second region would be preferred; this is clearly shown in Fig. 3(a), where the arrows show the tendency of inclination. For the $^2P^o(2)$ state, which has higher excitation energy, the distribution is more even along γ''. Nevertheless, in all the three $\pi(-1)^L=+1$ states, the preference for the first region is common.

For the $\pi(-1)^L=-1$ states, a typical example is the $^2D^o$ state. Here the third region is strongly preferred, as shown in Fig. 3(f); thus $\vec{r}_{12}$ is mostly parallel to the Z axis. For the $^4P^e$ and $^2P^e$ states, besides the third region, the fourth region is also non-negligible; this implies the tendency of rolling [shown by the arrows in Figs. 3(d) and 3(e)]. Nevertheless, in all the three $\pi(-1)^L=-1$ states, the preference for the third region is common.

VI. TWO-BODY DENSITIES

In order to understand the angles between a pair of electrons, we examine the polarity-dependent two-body densities $\tilde{\rho}_{\uparrow\uparrow}$ (dashed lines) and $\tilde{\rho}_{\uparrow\downarrow}$ (dotted lines) in Fig. 4 for the $\pi(-1)^L=+1$ states (upper frames) and $\pi(-1)^L=-1$ states (lower frames). The angles where each distribution arrives at the maximum values are denoted as $\bar{\theta}_{\uparrow\uparrow}$ and $\bar{\theta}_{\uparrow\downarrow}$, respectively, and their values are listed in Table II. Together with the distribution functions, we can arrive at the following conclusions:

(i) In all the $S=1/2$ states, $\tilde{\rho}_{\uparrow\uparrow}$ is different from $\tilde{\rho}_{\uparrow\downarrow}$; thus angular correlation between each pair of electrons depends on the spins.

(ii) Figures 4(a), 4(c), and 4(f) are similar in many respects. They all have only one peak in $\tilde{\rho}_{\uparrow\downarrow}$, implying that the down electron remains nearly equidistant from the two up electrons, resulting in an IST configuration. They all have $\bar{\theta}_{\uparrow\uparrow}$ larger than $\bar{\theta}_{\uparrow\downarrow}$; thus the IST is flattened with the two up electrons at the base. Thus, instead of an equilateral triangle, the IST arises because of the inequality of up-up and up-down angular correlations. If the wave function is sharply distributed around a coplanar structure, $\bar{\theta}_{\uparrow\uparrow}+2\times\bar{\theta}_{\uparrow\downarrow}$ should be close to 360°. However, in the $^2P^o$, $^2D^e$, and $^2P^e$ states, the above sums are equal to 324°, 328°, and 276°, respectively; thus the distribution around the coplanar structure is not sharp.

(iii) Figures 4(b) and 4(d) both have two peaks in $\tilde{\rho}_{\uparrow\downarrow}$; instead of an IST, this implies an irregular shape. The occurrence of this shape is due to a swing motion of the down electron, as will be shown later. In the $^2P^o(2)$ state, the $\bar{\theta}_{\uparrow\uparrow}$ is only 90°; thus the two up electrons are close to each other, resulting in a stronger Coulomb repulsion. In fact, among the eight intrashell states, this state is the highest.

(iv) Figures 4(e) and 4(g) show that $^4P^e$ and $^4S^o$ states are similar where $\tilde{\rho}_{\uparrow\uparrow}$ is identical to $\tilde{\rho}_{\uparrow\downarrow}$. The correlation in $S=3/2$ states is polarity independent. Since there is only one peak, the most probable shape is expected to be an equilateral triangle. The value $3\times\bar{\theta}_{\uparrow\uparrow}$ is a measure of how far the σ plane is shifted from the center. It is 330° in $^4P^e$, but 282° in $^4S^o$.

(v) Figure 4(h) for the $^2D^o$ state is distinctly different in that $\bar{\theta}_{\uparrow\downarrow}>\bar{\theta}_{\uparrow\uparrow}$. Thus instead of a flattened IST, it implies a prolonged IST. This state has been shown to tend toward the geometry shown in Fig. 1(b). The prolongation has the effect of increasing the moment of inertia to reduce the rotational kinetic energy.

VII. MODES OF INTERNAL MOTION

In order to study the internal motion let us define another body frame E'', so that $\vec{k}''$ is normal to σ, and the coordinates of e_1, e_2, and e_3 in the E'' frame read $(\theta,-\eta)$, (θ,η), and (θ,ϕ_3''), respectively. [This definition is slightly

TABLE II. The optimal angular separation (in degrees) where $\tilde{\rho}_{\uparrow\uparrow}$ and $\tilde{\rho}_{\uparrow\downarrow}$ are peaked. For the latter, the $^2P^o(2)$ and $^2S^e$ states have two peaks.

State	$^2P^o$	$^2P^o(2)$	$^2D^e$	$^2S^e$	$^4P^e$	$^2P^e$	$^4S^o$	$^2D^o$
$\tilde{\theta}_{\uparrow\uparrow}$	120	90	118	110	110	102	94	94
$\tilde{\theta}_{\uparrow\downarrow}$	102	78	105	63	110	87	94	117
		138		142				

different from that in (WL).] When $\theta=90°$, the σ plane contains the center; otherwise, the distance from σ to the center is $d=r_0\cos\theta$. In this frame, the internal motion can be classified into three basic modes (WL and Refs. [10,11]). One is associated with the variation of θ; in this mode all the electrons move in phase and the σ plane keeps its orientation but oscillates back and forth around the center, as intuitively shown in Fig. 5(a). It was called a d oscillation (d-OSC) mode, and the corresponding classical motion proved to be an exact periodic solution of Lagrange's equations [11].

The other two basic modes occur inside the σ plane; they can be called planar modes. One is associated with the variation of ϕ_3'', as intuitively shown in Fig. 5(b), where an electron swings back and forth with respect to the center of the other two. It is called a swing (SWI) mode [10]. The other one is associated with the variation of η, as intuitively shown in Fig. 5(c), where a pair of electrons oscillate relative to each other, while the third remains stationary. It is called an η-OSC mode [10].

It was shown in Ref. [10] that the $^2S^e$ state is dominated by the SWI mode; from the similarity of Figs. 4(b) and 4(d), it is expected that the $^2P^o(2)$ state would have a strong SWI motion as well. It was shown in Ref. [11] that the $^4S^o$ state is dominated by the d-OSC mode; since the σ planes in both the $^4S^o$ and $^2P^e$ states are shifted remarkably from the center [shown by Figs. 4(f) and 4(g)], the $^2P^e$ state is expected to also have strong d-OSC motion.

VIII. WAVE FUNCTIONS DISPLAYED IN THE E''-FRAME

We examine the modes of internal motion by displaying $f_{\frac{1}{2}\frac{1}{2}\frac{1}{2}}$ in the E'' frame. This function depends on θ,η,ϕ_3'' and the three Euler angles $\alpha'',\beta'',\gamma''$, where α'' will be given as zero. We again separate the states into $\pi(-1)^L=+1$ and -1 groups.

A. $\pi(-1)^L=+1$ states

These states have been shown to prefer the lying coplanar structures; thus the optimal case of $\beta''=0$, $\gamma''=0$, and $\theta=90°$ is chosen. With this choice, the three electrons are located in the fixed X-Y plane, and $\vec{r}_{12}$ is parallel to the Y axis. The real and the imaginary parts of $f_{\frac{1}{2}\frac{1}{2}\frac{1}{2}}$ as functions of η and ϕ_3'' are plotted in Fig. 6.

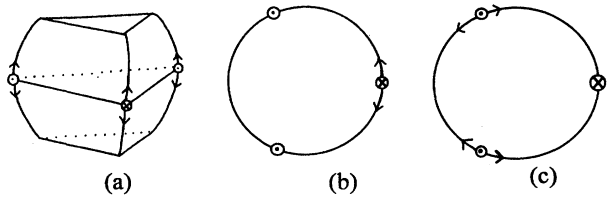

FIG. 5. Intuitive picture of the three basic modes of internal motion. (a) shows the d-OSC mode, (b) shows the SWI mode, and (c) shows the η-OSC mode. ⊙ and ⊗ label the up and down electrons, respectively.

1. The $^2P^o$ state (ground state)

The maximal magnitude of the real part is one order smaller than that of the imaginary part; thus only the latter is shown in Fig. 6(a). There is a peak at a flattened IST with base angle equal to 55°, and the wave function is smoothly distributed without any node. Incidentally, this state is dominated by the (ssp) angular momentum component with a weight of 90.6%. If we keep only the (ssp) component, then Fig. 6(a) is changed to Fig. 6(b), and the spatial correlation disappears. Thus, the independent-electron model fails in describing correctly the spatial correlation even in the ground state.

2. The $^2P^o(2)$ state

The maximal magnitude of the real part is close to that of the imaginary part. The real part is shown in Fig. 6(c), where the appearance of a peak and an antipeak implies a large-amplitude coplanar SWI oscillation. The imaginary part shown in Fig. 6(d) also has a nodal line, implying a large-amplitude η-OSC oscillation. These two energetic planar modes result in the loss of well-defined geometric structure for this state, as shown earlier.

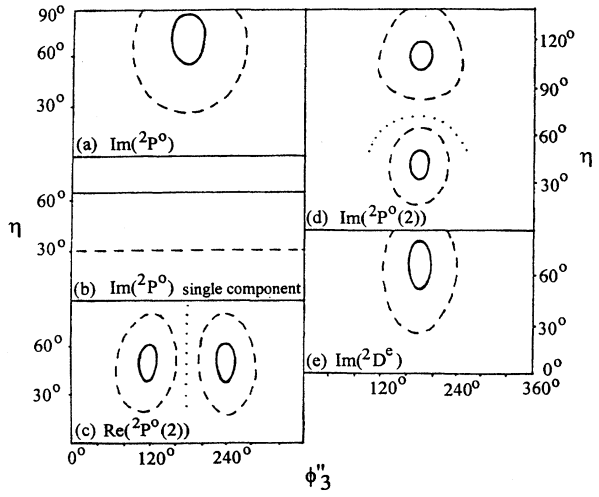

FIG. 6. The real or imaginary part of $f_{\frac{1}{2}\frac{1}{2}\frac{1}{2}}$ as a function of η and ϕ_3'', $\alpha''=0$, $\beta''=0$, $\gamma''=0$, and $\theta=90°$ are assumed. It is only plotted in the region of $\eta<\phi_3''<360°-\eta$. The full line gives $\pm 92\%$ of the maximal magnitude; the dashed line gives $\pm 48\%$. The dotted line is a nodal line.

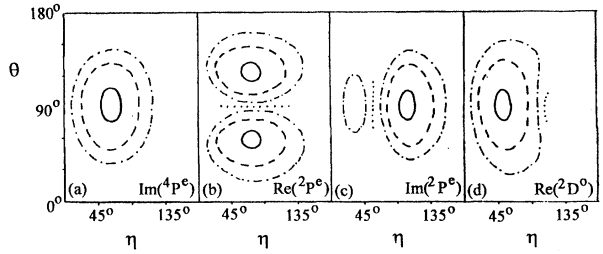

FIG. 7. The real or imaginary part of $f_{\frac{1}{2}\frac{1}{2}\frac{1}{2}}$ as a function of θ and η. $\alpha''=0$, $\beta''=90°$, $\gamma''=90°$, and $\phi_3''=180°$ are assumed. The full line gives $\pm 92\%$ of the maximal magnitude, the dashed line gives $\pm 48\%$, and the dashed-dotted line gives $\pm 20\%$. The dotted line is a nodal line.

3. The $^2D^e$ state

The maximal magnitude of the real part is one-half smaller than that of the imaginary part. The former contains a nodal line of the SWI mode, but because it is small, this SWI mode is not important. The imaginary part is shown in Fig. 6(e). There is a peak at a flattened IST with base angle equal to 57.5°. Thus, as predicted, the most probable shape is also a coplanar flattened IST just like the $^2P^o$ state. This similarity suggests that the $^2P^o$ and $^2D^e$ states belong to the same rotational band.

4. $^2S^e$ state

The state has been examined previously; [10] it has good coplanar structure with a strong SWI mode.

B. $\pi(-1)^L=-1$ states

Since these states prefer upstanding structures, the optimal case of $\beta''=90°$ and $\gamma''=90°$ is chosen and ϕ_3'' is given at a number of values. It was found that $\phi_3''=180°$ is the optimal case; thus only the results of this case are reported below. The real and the imaginary parts of $f_{\frac{1}{2}\frac{1}{2}\frac{1}{2}}$ as functions of θ and η are plotted in Fig. 7, where e_1 and e_2 are located symmetrically on the two sides of the fixed X-Y plane (above or below), e_3 is located in the X-Y plane so that the σ plane is parallel to the Y-Z plane; and the variation of θ is associated with a shift of the σ plane remaining parallel to the Y-Z plane.

1. The $^4P^e$ state

The maximal magnitude of the real part is one order smaller than the imaginary part; the latter is peaked at $\theta=90°$, $\eta=60°$, as shown in Fig. 7(a), which is associated with a coplanar upstanding ET. The appearance of the ET in $S=3/2$ states is natural because the up and down electrons are equal in the correlation.

2. The $^2P^e$ state

The maximal magnitude of the real part is close to that of the imaginary part. The real part is shown in Fig. 7(b), where the appearance of a peak and an antipeak implies a large-amplitude d-OSC. The imaginary part shown in Fig. 7(c) also has a nodal line; however, the antipeak is shallow and the gradient at the nodal line is small in magnitude; thus the associated η mode is less important. Hence, this state is dominated by the d-OSC mode; during this oscillation the σ planar remains upstanding.

3. The $^4S^o$ state

This state has been examined before [11]; it has a good ET structure with a strong d-OSC motion.

4. The $^2D^o$ state

The maximal magnitude of the real part is five times larger than that of the imaginary part; thus the former is dominant, which is peaked at $\theta=90°$, $\eta=48°$ and shown in Fig. 7(d). This state is similar to the $^4P^e$ state and the two states can be ascribed to the same rotational band.

IX. SUMMARY OF THE MAIN FEATURES

The main features are summarized in Table III. There are inherent relations among the features. For example, a strong d-OSC mode implies a noncoplanar structure; a strong SWI mode implies an irregular shape; a coexistence of different modes results in ambiguity in geometric structure; and the two $S=3/2$ head states have an ET shape.

X. FINAL REMARKS

The morphology (including the most probable shape, the most preferred orientation, and the preferred modes of internal motion) is a basic characteristic of bound quantum states, which has been investigated systematically via the observation of a number of correlation densities. In low-lying states, the morphology is decisively determined by the symmetry; in particular, by the structure of the INS in the multidimensional coordinate space, but not by the details of dynamics. This fact implies that similarity among different systems is widely established in nature [18]. In higher states, nodal surfaces of pure dynamical origin may appear [as in the $^2P^o(2)$ state]. The coupling of different basic modes is popular; accordingly, the morphology becomes complicated. Nonetheless, the existence of INS is always a basic factor in determining the structures. A systematic study of the morphology is essential in understanding the whole spectrum, and can provide a sound base for the classification of states.

Classifications of three-electron states have been attempted previously by Watanabe and Lin [7]. By expanding

$$\psi_{LM}(123)=\sum_Q D^L_{QM}(-\gamma,-\beta,-\alpha)\psi_{LQ}(1'2'3'), \qquad (17)$$

where the body frame is similar to the E'' frame (with a minor difference), it was suggested that Q can be defined as an approximate good quantum number. However, for the states examined there are strong mixings of the Q components, even in certain head states (e.g., in the $^2P^e$ state). Perhaps Q can be close to a better quantum number only in specific states. In this work, we do get a glimpse of states that display similar internal structure, and we have identified two pairs of states, where each pair may be viewed to form a rotational band (the $^2P^o$ and $^2D^e$ states and the $^4P^e$ and $^2D^o$ states, respectively).

TABLE III. Summary of the main features of intrashell three-electron states ($N=2$). The upper part is for $\pi(-1)^L=+1$, the lower for -1. CP means coplanar structure, $\approx$CP means a "a diffused distribution around a coplanar structure," NCP means noncoplanar structure. The orientation is relative to L. In $S=1/2$ states, the IST has the two spin-parallel electrons at the base. In the last column, a blank implies a small oscillation around the most probable shape without node; an unimportant mode is written within parentheses; e.g., the SWI mode in $^2D^e$.

State	Most probable shape	Coplanarity	Preferred orientation	Preferred modes(s)
$^2P^o$	Flattened IST	$\approx$CP	Lying or inclined	
	Base angle=55°			
$^2P^0(2)$	Not well defined	CP	Lying	SWI and η-OSC
$^2D^e$	Flattened IST	CP	Lying	(SWI)
	Base angle=57.5°			
$^2S^e$	Irregular triangle	CP	Isotropic	SWI
$^4P^e$	ET	$\approx$CP	Upstanding with rolling	
$^2P^e$	Not well defined	NCP	Upstanding with rolling	d-OSC (and η-OSC)
$^4S^o$	ET	NCP	Isotropic	d-OSC
$^2D^o$	Prolonged IST	$\approx$CP	Upstanding with $\vec{r}_{12}\|L$	(η-OSC)
	Base angle=66°			

In WL, the preferred modes of internal motion were not examined in great detail. The present work analyzes all the different modes as well as the preferential orientation and shapes. While it is not advisable to propose a complete classification scheme following the present limited analysis, this work is an effort in that direction. The morphology uncovered by this work provides a deeper understanding of the spectrum. It seems that the orientation (of the three-electron plane with respect to L) and the modes of motion (measured by the number of nodes in the basic modes) are important factors in classifying the states.

ACKNOWLEDGMENTS

This work is supported in part by the National Foundation of Natural Science of P.R. China and by the U.S. Department of Energy, Office of Basic Energy Research, Division of Chemical Sciences. C.G.B. thanks the Alexander von Humboldt Foundation for support.

[1] U. Fano, Rep. Prog. Phys. **46**, 97 (1983).
[2] R. Berry, G. S. Ezra, and G. Natanson, *New Horizons of Quantum Chemistry*, edited by P. O. Lowdin and B. Pullman (Reidel, Dordrecht, 1983), p. 77.
[3] A. R. P. Rau, *Atomic Physics*, edited by R. S. Van Dyck and E. N. Fortson (World Scientific, Singapore, 1984), Vol. 9.
[4] C. D. Lin, Adv. At. Mol. Phys. **22**, 77 (1986).
[5] C. D. Lin, in *Review of Fundamental Processes and Applications of Atoms and Ions*, edited by C. D. Lin (World Scientific, Singapore, 1993).
[6] K. H. Al-Bayati and K. E. Banyard, J. Phys. B **20**, 465 (1987).
[7] S. Watanabe and C. D. Lin, Phys. Rev. A **36**, 511 (1987).
[8] Y. Komninos, M. Chrysos, and C. A. Nicolaides, Phys. Rev. A **38**, 3182 (1988).
[9] K. T. Chung, Phys. Rev. A **44**, 5421 (1992); **45**, 7766 (1992); **46**, 6914 (1991).
[10] C. G. Bao, Z. Phys. D **22**, 557 (1992).
[11] C. G. Bao, J. Phys. B **25**, 3725 (1992).
[12] D. R. Herrick and O. Sinanoglu, Phys. Rev. A **11**, 97 (1975).
[13] J. M. Feagin and J. S. Briggs, Phys. Rev. Lett. **57**, 984 (1986).
[14] G. S. Ezra and R. S. Berry, Phys. Rev. A **28**, 1974 (1983).
[15] M. Karplus and R. N. Porter, *Atoms and Molecules* (Benjamin, New York, 1970).
[16] C. E. Moore, *Atomic Energy Levels*, Natl. Bur. Stand. (U.S.) Circ. No. 467 (U.S. GPO, Washington, D.C., 1949), Vol. I.
[17] C. A. Nicolaides, N. A. Piangos, and Y. Komninos, Phys. Rev. A **48**, 3578 (1993).
[18] C. G. Bao, Few-Body Syst. **13**, 41 (1992).
[19] C. G. Bao and W. Y. Ruan, Few-Body Syst. **15**, 25 (1993).
[20] C. G. Bao, J. Phys. B **26**, 4671 (1993).